INFLUENCE OF SPACE WEATHER CONDITIONS ON THE INTERMITTENCY OF THE *Pi*3 IRREGULAR GEOMAGNETIC PULSATIONS

© 2025 N. A. Kurazhkovskaya *, B. I. Klain, A.Yu. Kurazhkovskii *****

Borok Geophysical Observatory, Branch of the Schmidt Institute of Physics of the Earth, Russian Academy of Sciences (GO Borok IPE RAS), Borok (Yaroslavl oblast), Russia

**e-mail: knady@borok.yar.ru*

***e-mail: klain@borok.yar.ru*

****e-mail: ksasha@borok.yar.ru*

Received July 04, 2024

Revised September 04, 2024

Accepted September 26, 2024

Abstract. The influence of substorms intensity, solar wind and interplanetary magnetic field (IMF) parameters on the pattern of amplitude distributions (intermittency) of *Pi*3 pulsation bursts observed in the night sector of the magnetosphere during substorms development was studied. One-minute digital magnetic field observation data from Arctic and Antarctic observatories were used for the analysis (Heiss Island and Mirny). The index α, which reflects the slope of the cumulative distribution function of the *Pi*3 burst amplitudes, was considered as the main characteristic of the *Pi*3 pulsation intermittency. It was shown that the distributions of *Pi*3 burst amplitudes, depending on space weather conditions, obeyed different power laws. It was found that the α value in the northern and southern hemispheres was greater during the development of weak substorms than during the development of strong and moderate substorms. It was shown that the α values in the two hemispheres were comparable when Pi3 bursts were excited against the background of slow solar wind flows, at the northward direction of the IMF Bz component and at a high level of solar wind plasma turbulence. Under other analyzed conditions, an asymmetry in the change in the α index was found. It is assumed that the intermittency index α qualitatively characterizes the level of plasma turbulence in the region of excitation of Pi3 pulsation bursts.

Keywords: *high-latitude magnetosphere, geomagnetic pulsations, space weather, substorms, intermittency, turbulence*

DOI: 10.31857/S00167940250204e7

1. INTRODUCTION

As is known, irregular geomagnetic pulsations with periods > 150 c, which have the form of bursts with an unsteady frequency spectrum, belong to the Pi3 range [Pudovkin et al., 1976; Saito, 1978]. According to the classification [Saito, 1978], Pi3 pulsations are divided into two types according to the range of periods: Pip (T < 400 s) and Ps6 (T □ 400-600 s). However, researchers usually consider all long-period irregular pulsations observed in the night sector of the auroral zone and associated with the intensification of substorms as one type of Pi3, for example, [Nagano et al., 1981]. The intensity of Pi3 is significantly higher than that of other types of pulsations excited during substorms, and varies from tens to hundreds of Nt. One of the characteristic features of Pi3 pulsations is that they can be observed both very localized in latitude and globally over a wide range of latitudes and longitudes, for example [Kleimenova et al., 1998; Han et al., 2007].

Spatial-temporal, spectral, polarization, and other characteristics of pulsations *Pi* 3 are reflected in many publications, for example, [Suzuki et al., 1981; Matsuoka et al., 1995; Moiseev et al., 2020; Kurazhkovskaya and Kline, 2021; Martines-Bedenko et al., 2022]. Various possible mechanisms and excitation regions of irregular pulsations *Pi* 3 are discussed in the existing literature. Some studies [Han et al., 2007] even claim that the generation mechanisms of *Pi* 3 pulsations at different latitudes must be different. It is believed that the sources of *Pi* 3 can be located both on the dayside of the magnetosphere and on the nightside. For example, in [Han et al., 2007], it is suggested that global *Pi* 3 pulsations may be caused by impulsive changes in the solar wind dynamic pressure, and their source is the dayside of the magnetosphere. In several papers, for example, [Kleimenova et al., 1998; Kozyreva et al., 2009], the night ionosphere is considered as the source of excitation of latitudinally local irregular bursts of *Pi* 3. According to [Kleimenova et al., 1998], the intensification of large-scale three-dimensional electric currents in the ionosphere during the development of substorms on the nightside of the magnetosphere can lead to the generation of *Pi* 3. Synchronous observations of energetic electron precipitation, riometric absorption bursts, and geomagnetic pulsations in the *Pi* 3 range in the night sector of high latitudes indicate that the excitation region of *Pi* 3 is the ionosphere [Kozyreva et al., 2009]. The excitation of *Pi* 3 pulsations observed in polar caps is presumably associated by the authors [Yagova et al., 2004] with intermittent turbulence of the magnetosheath and oscillations of the magnetospheric tail lobes. The variety of sources of *Pi* 3 pulsations discussed in publications suggests that some aspects of the morphological patterns of this type of pulsations are still not fully investigated.

Previously, we [Kline et al., 2008; Kurazhkovskaya and Kline, 2021] have shown that the cumulative distribution function (*cumulative distribution function* -CDF) of the amplitudes of bursts *Pi3* , observed during the development of substorms in the night sector of the magnetosphere, follows a power law $f(A) = A^{-\alpha}$, where A is the amplitude of bursts, α is the exponent. Consequently, the *Pi* 3 pulsation bursts have intermittency properties. At the same time, the exponent α , reflecting the slope of the cumulative distribution function of burst amplitudes, can be considered as a characteristic of intermittency and the associated turbulence of the medium in which the bursts occur [Malinetsky and Potapov, 2000]. The question of whether the conditions of the interplanetary medium and the intensification of auroral processes affect the intermittency properties of *Pi* 3 pulsations, and, accordingly, the turbulence in the pulsation excitation region, remains open.

At the same time, it is known that the process of substorm development is closely related to space weather conditions, as evidenced by numerous publications, for example, [Tanskanen et al., 2011; Newell et al., 2013; Vorobyev et al., 2018]. The spectrum of heliosphere parameters and their combinations discussed in the literature in connection with the occurrence of substorms is quite wide. One of the most geoeffective parameters leading to the development of substorms and determining their intensity is certainly the vertical *Bz* component of the IMF [Akasofu, 1975]. In addition, the appearance and intensity of substorms depend on the direction of the *Bx* and *By* components of the IMF [Vorobyev et al., 2018; Kubyshkina et al., 2018]. The paper [Newell et al., 2016] shows a clear dependence of the probability of substorm occurrence on the solar wind speed. Other parameters, even if they do not lead to the development of substorms, have a certain influence on the processes of magnetosphere flow around by solar wind streams and on the penetration of energy into the magnetotail. The influence of space weather parameters on the morphology of substorms, apparently, cannot but affect the properties of *Pi* 3 pulsations, since the formation of their regime occurs during the development of substorms.

Due to the above and the close connection between *Pi* 3 pulsations and substorm development, it is interesting to investigate the influence of interplanetary medium parameters on the distribution patterns of *Pi* 3 burst amplitudes in the northern and southern hemispheres. The relevance of studying new features of *Pi* 3 pulsations increases also because geomagnetic field disturbances in the *Pi* 3 range, along with magnetic storms and substorms, can lead to the excitation of geoinduced currents, which are one of the space weather factors affecting power lines and other ground-based technological systems [Pilipenko et al., 2023]. In this work, we investigate the influence of substorm intensity, solar wind speed, and IMF components on the intermittency patterns of *Pi* 3 pulsations.

Additionally, we will examine the influence of the solar wind plasma beta parameter on the intermittency properties of *Pi* 3. The beta parameter equals the ratio of thermal pressure to magnetic pressure: $\beta = NkT/(B^2/8\pi)$, where N and T are the density (cm^{-3}) and temperature (°K) of the solar wind proton plasma, B is the magnitude of the interplanetary magnetic field (nT). It is known that the beta parameter is one of the parameters controlling the development of reconnection processes between interplanetary and geomagnetic fields and the turbulence state of the solar wind plasma [Phan et al., 2010; Wang et al., 2018]. Satellite observations have shown that at $0 < \beta \leq 1.3$, the solar wind plasma is highly turbulent, while at $\beta > 1.3$, it is weakly turbulent [Wang et al., 2018]. The influence of the solar wind beta parameter on the intermittency of *Pi* 3, which is related to plasma turbulence in the pulsation excitation region, has not been previously studied.

The purpose of this work is to investigate the influence of substorm intensity, solar wind speed, IMF component directions, and the beta parameter on the intermittency properties of irregular *Pi3* pulsations observed in high latitudes of the northern and southern hemispheres of Earth during substorm development.

2. DATA USED

The source material for the analysis of intermittency of Pi3 *Pi3* pulsation bursts was one-minute digital data of magnetic field observations from Arctic and Antarctic observatories: Hayes Island (code HIS, corrected geomagnetic coordinates $\Phi' = 74.80°$, $\Lambda' = 144.46°$) for the period 1997-1998 and Mirny (code MIR, corrected geomagnetic coordinates $\Phi' = -76.93°$, $\Lambda' = 122.92°$) for the period 1995-1998 from the World Data Center for Solar-Terrestrial Physics, Moscow (http://www.wdcb.ru/stp/data/geo_min.val/Variational_Measurements/Database_Earth_Magnetic_Field_Variations/). For the same period, hourly parameters of the solar wind and IMF were obtained from the OMNI 2 database (http://omniweb.gsfc.nasa.gov/ow.html). One-minute data of the *AL* -index and hourly values of the *AE* -index were taken from the World Data Centre for Geomagnetism, Kyoto (https://wdc.kugi.kyoto-u.ac.jp/wdc/Sec3.html). Additionally, the "Catalog of large-scale solar wind events for the period 1976-2002" (ftp://ftp.iki.rssi.ru/pub/omni/catalog/) was used, the description of which is provided in the work [Yermolaev et al., 2009].

As a characteristic of the intermittency of pulsations *Pi* 3, as in previous works [Kline et al., 2008; Kurazhkovskaya and Kline, 2021], we considered the index α , obtained by approximating the cumulative distribution function of the amplitudes of *Pi* 3 bursts with a power function. For each *Pi* 3 burst, the maximum amplitude (A) of the *Pi* 3 wave packet was considered, which was found

from the expression: $A = \sqrt{H^2 + D^2}$, where H and D are the maximum values of the meridional and azimuthal components of the magnetic field. The methodology for obtaining the index α is described in more detail in the work [Kurazhkovskaya and Kline, 2015]. In addition, for a preliminary comparative analysis of the properties of *Pi* 3 pulsations observed in the northern and southern hemispheres, the following characteristics were considered: 1) the duration of the *Pi* 3 pulsation wave packet - t ; 2) the maximum spectral density of individual *Pi* 3 bursts - S max; 3) the frequency corresponding to the maximum spectral density - f . Preliminary one-minute data from ground-based magnetic observations were filtered in the frequency band (1.2-3.4) mHz. Then, a spectral-temporal analysis of *Pi* 3 bursts was carried out based on the fast Fourier transform method. From the obtained amplitude spectra of *Pi* 3 bursts, the value of the maximum spectral density S max and the corresponding frequency f were estimated.

3. RESEARCH RESULTS

3.1. Comparison of characteristics of Pi3 pulsations observed at HIS and MIR

For this study, a list of observed Pi3 burst events was used *Pi* 3, which was compiled earlier in the work [Kurazhkovskaya and Kline, 2021]. For the analyzed periods, based on magnetic field registration data at HIS and MIR, 306 and 416 cases of *Pi* 3 bursts were studied, respectively. Before proceeding to the analysis of the intermittency properties of *Pi* 3 pulsations observed at HIS and MIR, let's compare some of their characteristics and morphological patterns at the two observatories. Figure 1 shows typical examples of *Pi* 3 pulsation bursts (H -component) observed at HIS – 9.11.1997 and MIR – 13.03.1995. The spectra of the analyzed pulsations over their observation time interval are shown on the right. The bottom part of the figure shows the dynamics of the *AL* -index, reflecting the intensity of the westward electrojet in the auroral zone. Typically, *Pi* 3 pulsations were observed against the background of negative bays in the dynamics of the *AL* -index lasting more than 20 minutes and with a minimum value of *AL* -index less than -100 nT, which corresponded to the development of magnetospheric substorms [Hsu and McPherron, 2007]. Thus, *Pi* 3 pulsations in both hemispheres were excited during the development of substorms in the night sector of the magnetosphere. During this time, the HIS and MIR observatories were located in the northern and southern polar cap regions. Further, a comparison of some characteristics of *Pi* 3 pulsations observed in the polar regions of the magnetosphere will be conducted. Typically, *Pi* 3 bursts observed in the northern and southern hemispheres had a drop-like shape. The average duration of *Pi* 3 bursts at HIS and MIR was approximately the same and amounted to $t \sim 65$ min.

The average amplitude of bursts at HIS (A = 440 nT) was significantly higher than at MIR (A = 302 nT).

Amplitude spectra of pulsations *Pi* 3, obtained during observation intervals of pulsations in HIS and MIR, had several peaks, which indicated a complex structure of oscillations. For each case of observation of pulsations *Pi* 3 in HIS and MIR, the spectral density of the main maximum S max and the frequency f, corresponding to it, were estimated from the spectra. Comparison of the spectral composition of oscillations *Pi* 3 (distributions of S max and f) in two hemispheres is presented in Fig. 2. The ranges of variation of the maximum spectral density of *Pi* 3 bursts in HIS and MIR were approximately similar and varied from 40-50 to 170 (in relative units). However, in the dominant number of cases, the value of the maximum spectral density of *Pi* 3 bursts in HIS was higher (S max = 100–110) than in MIR (S max = 90–100). The frequency of wave packets f, corresponding to S max, in HIS occupied the range from 1.2 to 3.0 mHz, and in MIR from 1.4 to 3.4 mHz. Bursts of *Pi* 3 with the highest spectral density were observed both in HIS and MIR predominantly at a frequency of f = 2.2–2.4 mHz.

3.2. Dependence of the frequency of observation of Pi3 pulsations in HIS and MIR on the maximum intensity of substorms.

As noted above, cases of recording *Pi* 3 in HIS and MIR were observed during substorm development in the night sector. Figure 3 shows the dependence of the frequency of Pi *Pi* 3 burst observations in HIS and MIR on the maximum intensity of substorms (*AE* max), characterized by the value of the *AE* -index. It can be seen that the intensity of substorms during which *Pi* 3 pulsations were observed varied over a wide range from 100 nT to 1000 nT and more. In HIS, *Pi* 3 pulsations were mainly observed during substorms with an intensity of 700-800 nT, while in MIR the value of *AE* max in the dominant number of cases was 500-600 nT. Usually, the *AL*− [Vorobyev et al., 2018] or *AE*− [Fu et al., 2021] indices are used to classify substorms by intensity. For example, according to [Fu et al., 2021], if the maximum value of the *AE* -index (*AE* max) of substorms belongs to the ranges 100 nT < *AE* max ≤ 500 nT, 500 nT < *AE* max ≤ 1000 nT or *AE* max > 1000 nT, then the substorms are considered weak, moderate, or strong, respectively. Judging by the distribution of *AE* max (Figure 3), in the northern and southern hemispheres, *Pi* 3 bursts were excited during weak and moderate as well as strong intensity substorms. Moreover, predominantly, *Pi* 3 bursts in both hemispheres were observed during the development of moderate substorms (43% in HIS and 48% of cases in MIR). The probability of observing *Pi* 3 pulsations during the development of weak substorms was slightly lower (38% in HIS and 36% of cases in

MIR). During the development of strong substorms, the fewest cases of *Pi* 3 pulsations were observed (18% in HIS and 16% in MIR). Thus, it can be noted that the excitation of *Pi* 3 bursts in the northern and southern hemispheres occurred mainly against the background of low and medium intensity substorms. The average amplitude of *Pi* 3 bursts increased with the intensity of substorms and was approximately twice as large during strong substorms compared to weak substorms.

3.3. Diurnal variations of Pi3 bursts in HIS and MIR .

Confirmation of the predominant appearance of *Pi* 3 pulsations in the night sector of the magnetosphere is their diurnal variation in observation frequency. Figure 4 shows the normalized to the maximum number of cases dependence of the observation frequency *N/N* max of *Pi* 3 bursts in HIS and MIR on local time. The most probable time for observing *Pi* 3 bursts in the two hemispheres occurs in the interval from evening to early morning hours. It can be seen that the diurnal variations of *Pi* 3 bursts in HIS and MIR are asymmetric relative to the midnight meridian. The distributions of *N/N* max in HIS and MIR are similar in shape but differ in the position of the observation frequency maxima. Thus, in HIS, the maximum observation frequency corresponds to post-midnight hours (00:00-01:00 MLT). In MIR, the maximum of the diurnal variation is observed in the pre-midnight hours (22:00-23:00 MLT).

3.4 . Dependence of Pi3 burst observation frequency in HIS and MIR on large-scale solar wind flows .

The paper [Despirak et al., 2019] shows that the occurrence of magnetospheric substorms is significantly influenced by large-scale structures of solar wind flows. Since the studied *Pi* 3 pulsations were observed in two observatories during substorm development, it seemed appropriate to determine during which types of solar wind flows they are excited. For this purpose, we used the "Catalog of large-scale solar wind phenomena for the period 1976-2002," which reflects both quasi-stationary and disturbed types of solar wind. We simultaneously compared the time intervals of *Pi* 3 pulsation registration in HIS and MIR with observations of various types of large-scale solar wind flows. The analysis results showed that *Pi* 3 bursts were observed in HIS and MIR against the background of seven types of large-scale solar wind structures. These structures are identified in the catalog [Yermolaev et al., 2009] as: 1) slow quasi-stationary plasma flow of solar wind from coronal streamers – SLOW; 2) high-speed solar wind flow from coronal holes – FAST; 3) coronal mass ejections (*Coronal Mass Ejection* – CME); 4) region of compressed plasma at the front of fast flows from polar coronal holes and slow flows from coronal streamers (*Corotating Interaction Region* – CIR); 5) compression region before the leading edge of the piston – SHEATH; 6) heliospheric

current sheet (*Heliospheric Current Sheet* – HCS); 7) magnetic clouds (*Magnetic Cloud* – MC). However, as shown in the histogram of the frequency of *Pi* 3 burst observations in two observatories depending on the above-listed types of solar wind flows (Fig. 5), the dominant part of *Pi* 3 bursts in HIS (33% of cases) was observed against the background of SLOW, and in MIR (39% of cases) against the background of FAST. The number of *Pi* 3 burst cases observed in HIS against the background of other flows was significantly less and amounted to: FAST – 21%, CME – 16%, CIR – 9%. In MIR, *Pi* 3 bursts were observed against the background of SLOW in 22% of cases, CME in 14% of cases, CIR in 11% of cases. Against the background of SHEATH, HCS, and MC, less than 10% of cases were observed in both HIS and MIR (Fig. 5).

Thus, comparing the characteristics of *Pi* 3 bursts observed in two hemispheres showed that they had approximately the same spectral composition and wave packet duration, but differed in amplitude levels, spectral density, and the intensity of substorms during which their predominant excitation occurred. Additionally, differences were revealed in diurnal variation and in the types of solar wind flows against which *Pi* 3 pulsations are excited.

Next, we will proceed to analyze the amplitude patterns of *Pi* 3 bursts observed at HIS and MIR depending on space weather conditions. Since substorms are one of the geomagnetic effects of space weather, we will initially consider the influence of substorm intensity on the intermittency of *Pi* 3 bursts.

3.5. Dependence of Pi 3 *burst intermittency at HIS and MIR on substorm intensity.*

As noted above, the intensity of substorms during the observation of *Pi* 3 pulsations varied over a wide range (Fig. 3). Using the substorm classification principle from [Fu et al., 2021], we divided all cases of *Pi* 3 bursts, both at HIS and MIR, into three clusters: *Pi* 3 pulsations excited during weak, moderate, and strong substorms. For each cluster, the nature of amplitude distributions of *Pi* 3 bursts observed in the two hemispheres was analyzed separately. Figure 6 shows the obtained amplitude distributions *N(A)* of *Pi* 3 bursts at HIS and MIR (black and gray curves, respectively). The right side of the figure shows the CDF of *Pi* 3 burst amplitudes at HIS and MIR (dark and light circles, respectively), starting from a certain threshold value A_0, on a logarithmic scale and their approximation by a power function. Black and gray lines correspond to the power law distribution of amplitudes of *Pi* 3 bursts observed at HIS and MIR, respectively. For ease of comparison of the intermittency properties of *Pi* 3 pulsations in the northern and southern hemispheres, the amplitude distributions and their CDF approximations are given in pairs (at HIS and MIR) on each graph.

As can be seen from Fig. 6, regardless of the substorm intensity, the amplitude distributions of pulsations *Pi* 3 in the northern and southern hemispheres have a non-Gaussian shape (with more pronounced distribution tails). Note that such distributions are called distributions with "heavy tails" (*heavy tails or fat tails*). Typically, the tails of such distributions are quite well approximated by a power function of the form: $f(x) = x^{-\alpha}$ (α - power exponent) for all x exceeding some threshold x_0 ($x > x_0$) [Malinetsky, Potapov, 2000]. With respect to pulsations *Pi* 3, the burst amplitude distributions for the three clusters, identified by substorm intensity, follow a power law $f(A) = A^{-\alpha}$, where A is the burst amplitude, α is the power exponent. However, the power laws in HIS and MIR, which govern the distributions of *Pi* 3 burst amplitudes, differ significantly, as evidenced by the different slopes of the approximating lines. One of the features of the obtained distributions is the significant difference in the value of the exponent α in HIS and MIR. In the northern hemisphere, the value of the exponent α is significantly lower than in the southern hemisphere ($\alpha_{HIS} < \alpha_{MIR}$), and sometimes can differ by approximately 2 times. Moreover, the values of the exponent α in HIS are lower than in MIR regardless of which cluster the pulsations *Pi* 3 belong to. Another feature of the obtained distributions is that both in HIS and MIR, the exponent α is larger in magnitude during weak substorms than during moderate and strong ones. Thus, in HIS, the intermittency exponent during weak substorms equals $\alpha = 1.75$, and during moderate and strong substorms $\alpha = 1.30$ and $\alpha = 1.55$ respectively. A similar trend in the change of parameter α is characteristic for cases of observation in *Pi3* in MIR. The value of the exponent α in MIR for the cluster of weak substorms is $\alpha = 3.50$, and for moderate and strong substorms $\alpha = 2.79$ and $\alpha = 3.05$ respectively.

3.6. Dependence of intermittency patterns of Pi 3 bursts in HIS and MIR on space weather conditions

The study of intermittency properties of *Pi* 3 pulsations depending on space weather conditions, similar to the previous section, is also based on dividing all analyzed cases into clusters. Thus, from Fig. 5 it follows that *Pi* 3 bursts in HIS and MIR are mainly observed during SLOW and FAST, respectively. According to the catalog [Yermolaev et al., 2009], plasma flows with velocity $V < 450$ km/s are considered as slow flows – SLOW, and flows with $V \geq 450$ km/s as fast flows – FAST. The study of the dependence of *Pi* 3 pulsation observation frequency on solar wind velocity showed that in HIS, 55% and 45% of *Pi* 3 pulsation cases were observed at $V < 450$ km/s and $V \geq 450$ km/s, respectively. In MIR, *Pi* 3 pulsations were predominantly (61% of cases) observed at $V \geq 450$ km/s, while at $V < 450$ km/s in MIR, only 39% of *Pi* 3 bursts were observed. In this regard, it

seems appropriate to compare the distribution patterns of burst *Pi* 3 amplitudes at each observatory for two clusters: *Pi* 3 bursts observed at $V < 450$ km/s and at $V \geq 450$ km/s.

Analysis of the IMF components behavior during *Pi* 3 burst observations showed that approximately 70% of *Pi3* cases in HIS and MIR were recorded at $Bz < 0$ and 30% at $Bz > 0$. *Pi* 3 pulsations in HIS and MIR were observed both at $Bx < 0$ (45% of cases) and $Bx > 0$ (55% of cases). Depending on the direction of the *By component* in 55% of cases, *Pi* 3 were observed at $By < 0$ and in 45% of cases at $By > 0$, both in HIS and MIR. The predominant observation of *Pi* 3 pulsations in both hemispheres at negative values of the *By component* of the IMF is a favorable condition for the generation of low and medium intensity substorms [Vorobyev et al., 2018]. Indeed, as follows from section 3.2 **.** , pulsations *Pi* 3 in HIS and MIR were observed against the background of weak and moderate substorms, which is consistent with the results of [Vorobyev et al., 2018]. Taking into account the direction of the IMF components, all cases of *Pi* 3 at each of the observatories were divided into 6 clusters depending on the sign of *Bx* -, *By* - and *Bz* - components of the IMF: bursts of *Pi* 3, observed at $Bx < 0$ and $Bx > 0$; $By < 0$ and $By > 0$; $Bz < 0$ and $Bz > 0$.

In order to determine the influence of solar wind plasma turbulence on the intermittency properties of *Pi* 3 bursts, the parameter β was used. According to the results of [Wang et al., 2018], there are two ranges of the solar wind parameter β variation: $0 < \beta \leq 1.3$ and $\beta > 1.3$, one of which reflects a high, the other a low degree of solar wind plasma turbulence. Based on the results of this work, all events of *Pi* 3 bursts in HIS and MIR were divided into two clusters: *Pi* 3 bursts observed at $0 < \beta \leq 1.3$ and $\beta > 1.3$. Thus, depending on the solar wind velocity, the direction of the IMF components, and the value of the β parameter, 10 clusters were formed. Taking into account the three clusters identified depending on substorm intensity, a total of 13 clusters were formed. For each cluster, a separate study of the CDF character of *Pi* 3 pulsation amplitudes was performed and estimates of the exponent ⟨ were obtained. Table 1 shows the cluster designations, the number of *Pi* 3 burst cases, their average amplitude, and the intermittency indices ⟨ obtained in each cluster.

Results of the analysis of the distribution of amplitudes of *Pi* 3 bursts depending on solar wind velocity, IMF component directions, and β parameter are presented in Figures 7-9. From the estimates of the exponent α , shown in the figures and Table 1, it follows that pulses of *Pi* 3 pulsations observed in HIS and MIR were always excited in a highly turbulent environment (the value of the exponent $\alpha > 1$ and in some cases was > 3). Regardless of the parameters considered (V , *Bx* -, *By* - and *Bz* - components of IMF, and β), the value of the exponent α in MIR was always greater than in HIS. The distributions of amplitudes of *Pi* 3 bursts in each cluster (at $V < 450$ km/s

and $V \geq 450$ km/s, $Bx < 0$ and $Bx > 0$; $By < 0$ and $By > 0$; $Bz < 0$ and $Bz > 0$, $0 < \beta \leq 1.3$ and at $\beta > 1.3$) obeyed, for the most part, different power laws. Nevertheless, in 3 out of 10 clusters, a similarity in the slope of the approximating lines in the Northern and Southern hemispheres is found. For example, with slow solar wind ($V < 450$ km/s), the distribution of amplitudes of *Pi* 3 bursts is such that in HIS and MIR, the approximating lines are practically parallel to each other and the exponents α are close in magnitude (Fig. 7). Similar behavior of the slope of approximating lines in the two hemispheres is observed at $Bz > 0$ and $0 < \beta \leq 1.3$ (Fig. 8 and Fig. 9). Unexpectedly, there was a similarity in power laws in HIS and MIR at $0<\beta\leq 1.3$, i.e., when the solar wind plasma is highly turbulent. In this case, the exponent value $\alpha_{HIS} = \alpha_{MIR} = 2.56$.

The asymmetric behavior of the index α in the two hemispheres is noteworthy, depending on almost all parameters. Thus, in HIS, the value of the index α is higher during slow solar wind flow ($V < 450$ km/s) than during fast flow ($V \geq 450$ km/s), and equals 2.02 and 1.21 respectively. In MIR, the opposite trend is observed: the amplitude distribution of *Pi* 3 bursts observed during FAST was approximated by a power function with a higher index α (3.16) than during SLOW (2.69). Also, asymmetric behavior of α in the two hemispheres of the magnetosphere is typical for different directions of the radial and vertical components of the IMF. If in HIS at $Bx < 0$ and $Bz < 0$ the value of α is lower than at $Bx > 0$ and $Bz > 0$, then in MIR, conversely, when these IMF components are positive, the index α is lower than when they are negative. In HIS, the value of the index α during strong solar wind turbulence ($0 < \beta \leq 1.3$) is higher than during weak turbulence ($\beta > 1.3$) and equals 2.56 and 1.63 respectively. In MIR, during weak solar wind turbulence, the index α is higher (3.90) than during strong solar wind turbulence (2.56). The exception is the dependence of the character of amplitude distributions of *Pi* 3 bursts on the sign of the *By* -component of the IMF. The trend of α behavior at $By < 0$ and $By > 0$ in the two hemispheres is similar. At $By < 0$, the index α in HIS and MIR equals 1.49 and 2.34 respectively, which is lower than at $By > 0$ (1.79 and 3.24). Thus, under conditions of $V \geq 450$ km/s, $Bz < 0$, $Bx < 0$, $Bx > 0$, $\beta > 1.3$, a clear difference in the power laws of amplitude distributions of *Pi* 3 bursts in the two hemispheres and, accordingly, a difference in intermittency indices was observed.

4. DISCUSSION

This paper compares some morphological patterns of *Pi* 3 pulsations and analyzes their intermittency properties based on observational data from two Arctic and Antarctic observatories located in approximately conjugate regions. The HIS and MIR observatories are offset from each

other by only ~ one time zone in geomagnetic longitude and by ~ two degrees in geomagnetic latitude. Based on the location of the observatories in quasi-conjugate regions of the magnetosphere, similarities were expected in both morphological characteristics and intermittency patterns of *Pi* 3 pulsations in the northern and southern hemispheres. However, as a result of comparative analysis of *Pi* 3 pulsations recorded at HIS and MIR, both similar and different patterns were identified. For instance, at HIS and MIR, *Pi* 3 pulsations had approximately the same spectral composition and average duration of wave packets. In the northern and southern hemispheres, *Pi* 3 bursts were observed in the night sector of polar latitudes primarily during the development of moderate substorms (500 nT < *AE* max ≤ 1000 nT). In addition, the excitation of *Pi* 3 bursts occurred under some similar heliospheric parameters. For example, the highest probability of *Pi* 3 bursts in both hemispheres was observed with the same direction of IMF components ($Bz < 0$, $Bx > 0$ and $By < 0$). Also, *Pi* 3 bursts at both HIS and MIR were observed in the dominant number of cases when the parameter $\beta > 1.3$ (with relatively weak solar wind turbulence).

According to the results of [Kurazhkovskaya and Klein, 2021], pulsations *Pi* 3 have elliptical polarization. In this regard, pulsations *Pi* 3 can be identified with Alfvén waves propagating along the Earth's external magnetic field. A suitable model for such waves can be the nonlinear Schrödinger equation [Zakharov et al., 1988]:

$$\psi_t + \psi_{xx} + R(|\psi|^2)\psi = 0 \qquad (1)$$

A simple model that takes into account the main features of equation (1) is based on the principles of implementing switching intermittency [Bartucelli et al., 1990; Malinetsky and Potapov, 2000]. The main conclusions of these works reduce to the fact that the probability density of amplitude bursts, as in the work of [Zakharov et al., 1988], is characterized by a power-law asymptotic: $f(A) = A^{-\alpha}$. When studying the nature of amplitude distributions of pulsations *Pi* 3, we accepted this fact as a hypothesis.

The conducted study showed that in both hemispheres, the amplitude distributions of *Pi* 3 bursts, regardless of space weather conditions, followed a power law. Typically, in the northern and southern hemispheres, the values of intermittency indices α were > 1 and in some cases > 3. Consequently, *Pi* 3 bursts in both hemispheres were excited in a highly turbulent environment [Malinetsky and Potapov, 2000]. Under certain space weather conditions, the slopes of the lines approximating the CDF of *Pi* 3 burst amplitudes were similar in both hemispheres, and the intermittency indices α were practically equal in magnitude. This means that the amplitude distributions of *Pi* 3 bursts in the two hemispheres are characterized by approximately similar power

laws. For example, under interplanetary conditions $V < 450$ km/s, $Bz > 0$ and $0 < \beta \leq 1.3$, the values of intermittency indices in HIS and MIR differed insignificantly. Based on this, it can be assumed that during slow solar wind, in the absence of reconnection processes at the front boundary of the magnetosphere, and with a high level of solar wind plasma turbulence, *Pi* 3 bursts were excited in both hemispheres in an environment with approximately the same turbulence. In other words, under these conditions, the properties of intermittency were practically symmetric in the two hemispheres. Since the CDF of *Pi* 3 burst amplitudes at $V < 450$ km/s, $Bz > 0$ and $0 < \beta \leq 1.3$ followed approximately the same power laws, they could penetrate from a single source into the northern and southern hemispheres and have identical generation mechanisms. Judging by the diurnal variation in the frequency of *Pi* 3 pulsation observations and their close connection with substorms, the excitation region of *Pi* 3 pulsations is presumably located in the magnetospheric tail, the plasma of which is highly turbulent [Budaev et al., 2011; Levashov et al., 2022].

However, besides the similarity of Pi *Pi* 3 burst characteristics in the two hemispheres, there were also significant differences between them. The Pi *Pi* 3 pulsations in HIS and MIR differed in terms of average amplitude levels and spectral density values (Fig. 2). Generally, the average amplitude and spectral density of Pi *Pi* 3 bursts in the northern hemisphere were higher than in the southern hemisphere. Differences were identified in the diurnal variation of the Pi *Pi* 3 burst observation frequency by local magnetic time. In the northern hemisphere, Pi *Pi* 3 bursts appeared more frequently after midnight, while in the southern hemisphere they occurred before midnight (Fig. 4). Pi *Pi* 3 bursts were generated in HIS and MIR against the background of different types of large-scale solar wind flows (Fig. 5).

Power laws in HIS and MIR, which govern the amplitude distributions of Pi *Pi* 3 bursts, varied significantly depending on the substorm type, as well as on the direction of the IMF components (except for the condition $Bz > 0$) and on the value of the β parameter (specifically at $\beta > 1.3$), as evidenced by different slopes of the approximating lines. It is shown that at $V \geq 450$ km/s, $Bz < 0$, $Bx < 0$, $Bx > 0$, $\beta > 1.3$, there was asymmetry in both hemispheres of the magnetosphere in the behavior of the index α . Depending on the direction of the *By* -component, no differences in the trend of the index α behavior in HIS and MIR were revealed. Due to the tendency of the CDF of Pi *Pi* 3 amplitudes to follow different power laws, there is reason to believe that Pi *Pi* 3 bursts may have different origins in the two hemispheres and possibly different generation mechanisms.

The obtained results allow for a qualitative assessment of the plasma turbulence degree in the excitation region of pulsations *Pi* 3. Thus, based on the results presented in Fig. 6, it can be assumed

that during substorm development, the plasma in the generation region of pulsations *Pi* 3 is more turbulent in the southern hemisphere than in the northern one. One explanation for the observed differences in turbulence degree in the excitation region of pulsations *Pi* 3 may be their association with different types of substorms. According to [Kleimenova et al., 2012], polar and high-latitude substorms are distinguished. In [Despirak et al., 2019], it is shown that polar and high-latitude substorms are observed under different solar wind conditions. Polar substorms are observed at geomagnetic latitudes > 70° ° predominantly during SLOW ($V < 450$ km/s). High-latitude substorms (analogous to classical substorms), being excited at latitudes < 70° ° , move into the polar cap region, and are observed mainly during FAST ($V \geq 450$ km/s). It is possible that in HIS, the excitation of *Pi* 3 bursts is associated with polar substorms, while in MIR with high-latitude ones, since the probability of observing both types of substorms and *Pi* 3 bursts depending on the type of solar wind flows coincides. Based on the obtained results, a higher level of plasma turbulence should be expected in the excitation region of pulsations *Pi* 3 during the development of classical substorms than during polar substorms.

Some morphological differences and intermittency features of *Pi* 3 bursts observed in the two hemispheres may also be due to topological features of the magnetosphere, since the location of HIS and MIR observatories is such that there is a small shift between them in geomagnetic latitude and longitude. Another factor influencing the difference in properties of *Pi* 3 bursts may be the specifics of the solar wind flow around the northern and southern hemispheres of Earth.

However, it is not always possible to offer an explanation for the observed patterns of intermittency of pulsations *Pi* 3 . So, it is unclear why the turbulence level in the generation region of *Pi* 3 bursts in the two hemispheres is highest during the development of weak storms? Why does the high turbulence of the solar wind (at $0 < \beta \leq 1.3$) similarly affect the turbulence of the medium in which *Pi* 3 bursts are excited in the northern and southern hemispheres. At the same time, the influence of weak solar wind turbulence ($\beta > 1.3$) differs in the two hemispheres.

In conclusion, it should be noted that the patterns of intermittency are also characteristic of the substorms themselves. For example, in the work [Dobias and Wanliss, 2009] it is noted that *AE* - and *AL* - indices follow a power law, and the intervals between the peaks of the *AE* -index are distributed exponentially [Consolini and Michelis, 2002]. According to [Malinetsky and Potapov, 2000], the power-law distribution of peak amplitudes and the exponential distribution of inter-peak intervals are the main signs of intermittency. Consequently, the process of substorm generation itself has an intermittent nature, which also indicates the turbulence of the magnetospheric tail plasma. In

connection with the above, ground-based observations of *Pi* 3 pulsations can be used for qualitative assessment of the plasma turbulence in the magnetospheric tail depending on the changing space weather conditions during the development of substorms of various intensities.

5. CONCLUSION

The influence of substorm intensity, solar wind parameters, and interplanetary magnetic field on the intermittency patterns of *Pi* 3 pulsation bursts observed in the night sector of the magnetosphere during substorm development has been investigated. Similar and different morphological patterns, as well as intermittency properties of *Pi* 3 bursts observed in the northern and southern hemispheres, have been discovered. In HIS and MIR, *Pi* 3 pulsations were observed in the night sector of polar latitudes predominantly during substorm development, had approximately the same spectral composition and average duration of wave packets. Analysis of interplanetary medium parameters showed that excitation of *Pi* 3 bursts occurred predominantly with the same IMF direction ($Bz < 0$, $Bx > 0$ and $By < 0$) and with a parameter value $\beta > 1.3$ in both hemispheres.

Pulsations *Pi* 3 in HIS and MIR differed significantly in terms of average amplitudes and spectral density. Differences were revealed in the diurnal variation of the frequency of Pi 3 burst observations by local magnetic time. It is shown that the distributions of *Pi* 3 burst amplitudes depending on substorm intensity, solar wind speed, IMF component directions, and the value of the β parameter followed power laws with an intermittency index *Pi* 3 ⌈ exceeding 1. The latter indicated that *Pi* 3 pulsation bursts in both hemispheres were excited in a highly turbulent environment. The value of the index ⌈ in both HIS and MIR was higher during the development of weak substorms compared to moderate and strong intensity substorms. The intermittency indices $⌈_{HIS}$ and $⌈_{MIR}$ were comparable in magnitude when *Pi* 3 bursts were excited against the background of slow solar wind flows ($V < 450$ km/s), with a northward direction of the vertical IMF component ($Bz > 0$) and $0 < \beta \leq 1.3$. An asymmetry was discovered in the change of the index ⌈ in the northern and southern hemispheres at $V \geq 450$ km/s, $Bx < 0$, $Bx > 0$, $Bz \leq 0$, $\beta > 1.3$. Depending on the direction of the By -component, no differences in the behavioral trend of the index ⌈ in HIS and MIR were revealed. The discovered patterns of *Pi* 3 burst intermittency can be used for qualitative assessment of the degree of plasma turbulence in the magnetospheric tail (which is presumably the excitation region of these pulsations) depending on space weather conditions. It is assumed that in the northern hemisphere, plasma turbulence in the *Pi* 3 burst excitation region is higher at $V < 450$

km/s, $Bx > 0$, $Bz \geq 0$, $0 < \beta \leq 1.3$, while in the southern hemisphere, on the contrary, at $V \geq 450$ km/s, $Bx < 0$, $Bz \leq 0$, $\beta > 1.3$.

ACKNOWLEDGMENTS

The authors express their gratitude to the staff of the World Data Center for Solar-Terrestrial Physics (Moscow) for the opportunity to use geomagnetic data from the Hayes Island and Mirny observatories, to the creators of the OMNI 2 database (Goddard Space Flight Center, NASA, USA), World Data Centre for Geomagnetism (Kyoto), and to the authors of the "Catalog of large-scale solar wind phenomena for the period 1976-2002" (IKI RAS, Moscow) for the possibility to use these data.

FUNDING

The work was carried out within the framework of the State assignment of the Geophysical Observatory "Borok" IPE RAS. State assignment No. FMWU-2022-0027.

REFERENCES

– *Budaev V.P., Savin S.P., Zelenyi L.M* . Observation of intermittency and generalized self-similarity in turbulent boundary layers of laboratory and magnetospheric plasma: towards determining quantitative characteristics of transport // UFN. Vol. 18. No. 9. P. 905–952. 2011. https://doi.org/10.3367/UFNr.0181.201109a.0905

– *Vorobyev V.G., Yagodkina O.I., Antonova E.E., Zverev V.L.* Influence of solar wind plasma parameters on the intensity of isolated magnetospheric substorms // Geomagnetism and Aeronomy. Vol. 58. No. 3. P. 311–323. 2018. https://doi.org/10.7868/S001679401803001X

– *Despirak I.V., Lyubchich A.A., Kleimenova N.G.* Different types of solar wind streams and substorms at high latitudes // Geomagnetism and Aeronomy. Vol. 59. No. 1. P. 3–9. 2019. https://doi.org/10.1134/S001679401901005X

– *Yermolaev Yu.I., Nikolaeva N.S., Lodkina I.G., Yermolaev M.Yu.* Catalog of large-scale solar wind phenomena for the period 1976-2000 // Cosmic Research. Vol. 47. No. 2. P. 99–113. 2009.

– *Zakharov V.E., Pushkarev A.N., Shvets V.F., Yankov V.V.* On soliton turbulence // JETP Letters. Vol. 48. Issue 2. P. 79–82. 1988.

– *Kline B.I.* , *Kurazhkovskaya N.A.* , *Kurazhkovsky A.Yu.* Intermittency in wave processes // Physics of the Earth. No. 10. P. 25–34. 2008.

– *Kleimenova N.G., Kozyreva O.V., Bitterly J., Bitterly M.* Long-period (T=8 - 10 min) geomagnetic pulsations at high latitudes // Geomagnetism and Aeronomy. Vol. 38. No. 4. P. 38–48. 1998.
– *Kleimenova N.G., Antonova E.E., Kozyreva O.V., Malysheva L.M., Kornilova T.A., Kornilov I.A.* Wave structure of magnetic substorms at polar latitudes // Geomagnetism and Aeronomy. Vol. 52. No. 6. P. 785–793. 2012.
– *Kozyreva O.V., Myagkova I.N., Antonova E.E., Kleimenova N.G.* Precipitation of energetic electrons and Pi3 geomagnetic pulsations at polar latitudes // Geomagnetism and Aeronomy. Vol. 49. No. 6. P. 777–785. 2009.
– *Kurazhkovskaya N.A., Kline B.I.* Influence of geomagnetic activity, solar wind parameters, and interplanetary magnetic field (IMF) on the patterns of intermittency of Pi2 geomagnetic pulsations // Solar-Terrestrial Physics. Vol. 1. No. 3. P. 11–20. 2015. https://doi.org/10.12737/11551
– *Kurazhkovskaya N.A., Kline B.I.* Polarization characteristics of high-latitude Pi3 geomagnetic pulsations // Geomagnetism and Aeronomy. Vol. 61. No. 2. P. 195–210. 2021. https://doi.org/10.31857/S0016794021010107
– *Levashov N.N., Popov V.Yu., Malova Kh.V., Zelenyi L.M* . Modeling of intermittent turbulence in space plasma // Cosmic Research. Vol. 60. No. 1. P. 11–16. 2022. https://doi.org/10.31857/S0023420622010083
– *Malinetskiy G.G., Potapov A.B.* Modern problems of nonlinear dynamics. Moscow: Editorial URSS, 335p. 2000.
– *Moiseev A.V., Starodubtsev S.A., Mishin V.V.* Features of excitation and propagation along azimuth and meridian of long-period *Pi* 3 oscillations of the geomagnetic field on December 8, 2017 // Solar-Terrestrial Physics. Vol. 6. No. 3. P. 56–72. 2020. https://doi.org/10.12737/szf-63202007
– *Pudovkin M.I., Raspopov O.M., Kleimenova N.G.* Disturbances of the Earth's electromagnetic field. Part II. Short-period oscillations of the geomagnetic field. Leningrad: Leningrad State University Publishing House, 271 p. 1976.
– *Akasofu S.I.* Roles of north-south component of interplanetary magnetic-field on large-scale auroral dynamics observed by DMSP satellite // Planetary and Space Science. V. 23.N. 10. P. 1349–1354. 1975. https://doi.org/ 10.1016/0032-0633(75)90030-6
– *Bartucelli M., Constantin P., Doering C.R., Gibbon J. D., Gisselfält M.* On the possibility of soft and hard turbulence in the complex Ginzburg-Landau equation // Physica D. V. 44. P. 421–444. 1990.

https://doi.org/10.1016/0167-2789(90)90156-J

– *Consolini G., De Michelis P.* Fractal time statistics of *AE* index burst waiting times: evidence of metastability // Nonlinear Processes in Geophysics. V. 9. P. 419–423. 2002. https://doi.org/10.5194/npg-9-419-2002

– *Dobias P., Wanliss J.A.* Intermittency of storms and substorms: is it related to the critical behaviour? // Ann. Geophys. V. 27. P. 2001–2018. 2009. https://doi.org/10.5194/angeo-27-2011-2009

– *Fu H., Yue C., Zong Q.-G., Zhou X.-Z., Fu S* . Statistical characteristics of substorms with different intensity // J. Geophys. Res.: Space Physics. V. 126, e2021JA029318. 2021. https://doi.org/10.1029/2021JA029318

– *Han D.-S., Yang H.-G., Chen Z.-T., Araki T., Dunlop M.W., Nosé M., Iyemori T., Li Q., Gao Y.-F., Yumoto K.* Coupling of perturbations in the solar wind density to global *Pi* 3 pulsations: A case study // J. Geophys. Res. V. 112. A05217. 2007. https://doi.org/10.1029/2006JA011675

– *Hsu T.-S., McPherron R.L.* A statistical study of the relation of *Pi* 2 and plasma flows in the tail // J. Geophys. Res. V. 112. A05209. 2007. https://doi.org/10.1029/2006JA011782

– *Kubyshkina M., Semenov V., Erkaev N., Gordeev E., Dubyagin S., Ganushkina N., Shukhtina, M.* Relations between *vz* and *Bx* components in solar wind and their effect on substorm onset // GRL. V. 45. 2018. https://doi.org/10.1002/2017GL076268

– *Martines-Bedenko V.A., Pilipenko V.A., Hartinger M., Partamies N.* Conjugate properties of *Pi* 3/ *Ps* 6 pulsations according to Antarctica-Greenland observations // Russian Journal of Earth Sciences. V. 22. ES4006. 2022. https://doi.org/10.2205/2022ES000805

– *Matsuoka H., Takahashi K., Yumoto K., Anderson B.J., Sibeck D.G* . Observation and modeling of compressional *Pi* 3 magnetic pulsations // J. Geophys. Res. V. 100. № A7. P. 12103–12115. 1995. https://doi.org/10.1029/94JA03368

– *Nagano H., Suzuki A.* , *Kim* J. *S. Pi* 3 magnetic pulsations associated with substorms // Space Sci. V. 29. №. 5. P. 529–553. 1981. https://doi.org/10.1016/0032-0633(81)90067-2

– *Newell P.T., Gjerloev J.W., and Mitchell E.J.* Space climate implications from substorm frequency // J. Geophys. Res. Space Physics. V. 118. P. 6254–6265. 2013. https://doi.org/10.1002/jgra.50597

– *Newell P.T., Liou K., Gjeroev J.W., Sotirelis T., Wing S., Mitchell E.J.* Substorm probabilities are best predicted from solar wind speed // J. Atmos. Solar-Terr. Phys. V.146. P. 28–37. 2016. https://doi.org/10.1016/j.jastp.2016.04.019

– *Phan T.D., Gosling J.T., Paschmann G., Pasma C., Drake J.F, Øieroset M., Larson D., Lin R.P., Davis M.S.* The dependence of magnetic reconnection on plasma β and magnetic shear evidence

from solar wind observation // Astrophys J. Lett. V. 719 :L199-L203. 2010. https://doi.org/10.1088/2041-8205/719/2/L199

– *Pilipenko V., Kozyreva O., Hartinger M., Rastaetter L., Sakharov Y* . Is the global MHD modeling of the magnetosphere adequate for GIC prediction: the May 27–28, 2017 storm // Cosmic Research. V. 61. № 2. P. 120–132. 2023. https://doi.org/10.1134/S0010952522600044

– *Saito T.* Long period irregular magnetic pulsations Pi3 // Space Sci. Rev. V. 21. P. 427–467. 1978. https://doi.org/10.1007/BF00173068

– *Suzuki A., Nagano H., Kim J.S.* A statistical study on characteristics of high latitude Pi3 pulsations // J. Geophys. Res. V. 86. № A3. P. 1345–11354. 1981. https://doi.org/10.1029/JA086iA03p01345

– *Tanskanen E.I., Pulkkinen T. I., Viljanen A., Mursula K., Partamies N., Slavin J. A.* From space weather toward space climate time scales: Substorm analysis from 1993 to 2008 // J. Geophys. Res. V. 116. A00I34. 2011. https://doi.org/10.1029/2010JA015788

– *Yagova N.V., Pilipenko V.A., Lanzerotti L.J., Engebretson M.J., Rodger A.S., Lepidi S., Papitashvili V.O.* Two-dimensional structure of long-period pulsations at polar latitudes in Antarctica // J. Geophys. Res. V. 109 . A03222. 2004. https://doi.org/10.1029/2003JA010166

– *Wang X., Tu C.-Y., He J.-S., Wang L.-H.* Ion-scale spectral break in the normal plasma beta range in the solar wind turbulence // J. Geophys. Res.: Space Physics. V. 123. P. 68–75. 2018. https://doi.org/10.1002/2017JA024813

Table 1. Estimates of the mean values of the amplitudes of *Pi* 3 bursts and the intermittency index α in HIS and MIR depending on the intensity of substorms and parameters of solar wind and IMF

	HIS			MIR		
Parameter	*N*	*A* , nT	α	*N*	*A* , nT	α
100 nT < *AE* ≤500 nT	118	340	1.75	147	218	3.50
500 nT < *AE* ≤1000 nT	131	459	1.30	198	317	2.79
AE >1000 nT	55	618	1.55	66	454	3.05
V < 450 km/s	166	342	2.02	162	201	2.69
V ≥ 450 km/s	137	548	1.21	251	368	3.16
Bx < 0	136	444	1.63	186	299	2.92
Bx ≥ 0	168	429	1.70	227	306	2.34
By < 0	168	468	1.49	231	303	2.34
By ≥ 0	136	396	1.79	182	303	3.24
Bz < 0	221	462	1.38	288	324	3.00
Bz ≥ 0	83	364	2.30	125	253	2.48
0 < β ≤ 1.3	134	413	3.56	157	294	2.56
β > 1.3	169	453	1.65	255	308	3.90

FIGURE CAPTIONS

Fig. 1. Typical examples of *Pi* 3 pulsations observation (*H* component) at Hayes Island observatory (9.11.1997) and Mirny (13.03.1995). On the right, amplitude spectra of *Pi* 3 pulsations are shown for the interval of their observation. Below is the dynamics of the *AL* -index.

Fig. 2. Dependence of observation frequency *N* of pulsations *Pi* 3 in HIS and MIR on the maximum spectral density of wave packets *S* max and its corresponding frequency *f* .

Fig. 3. Dependence of observation frequency *N* of pulsations *Pi* 3 in HIS and MIR on the maximum substorm intensity, characterized by the value of *AE* -index.

Fig. 4. Diurnal variation of observation frequency, normalized to the maximum number of cases *N* / *N* max of pulsations *Pi* 3 in HIS and MIR.

Fig. 5. Distribution of occurrence frequency *N* of pulsations *Pi* 3 in HIS and MIR depending on large-scale solar wind flows.

Fig. 6. Dependence of intermittency of pulsations *Pi* 3 in HIS and MIR on the maximum substorm intensity. The left shows distributions *N(A)* of amplitudes of pulsation bursts *Pi* 3 in HIS (black curve) and MIR (gray curve). The right shows cumulative distribution functions CDF of pulsation amplitudes *Pi* 3 in HIS and MIR (dark and light circles respectively) and their approximation by a power function (black and gray lines respectively).

Fig. 7. Dependence of intermittency of pulsations *Pi* 3 in HIS and MIR on the velocity of slow and fast solar wind flows. Notations are the same as in Fig. 6.

Fig. 8. Dependence of intermittency of pulsations *Pi* 3 in HIS and MIR on the direction of *Bx* -, *By* - and *Bz* - components of IMF. Notations are the same as in Fig. 6.

Fig. 9. Dependence of intermittency of pulsations *Pi* 3 in HIS and MIR on the value of plasma parameter β . Notations are the same as in Fig. 6.

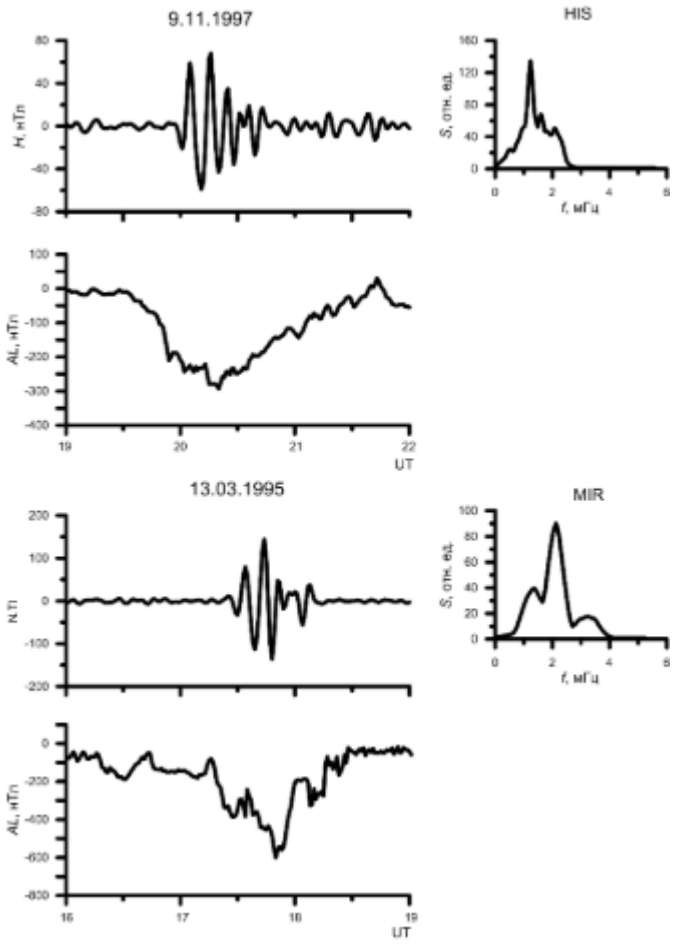

Fig. 1.

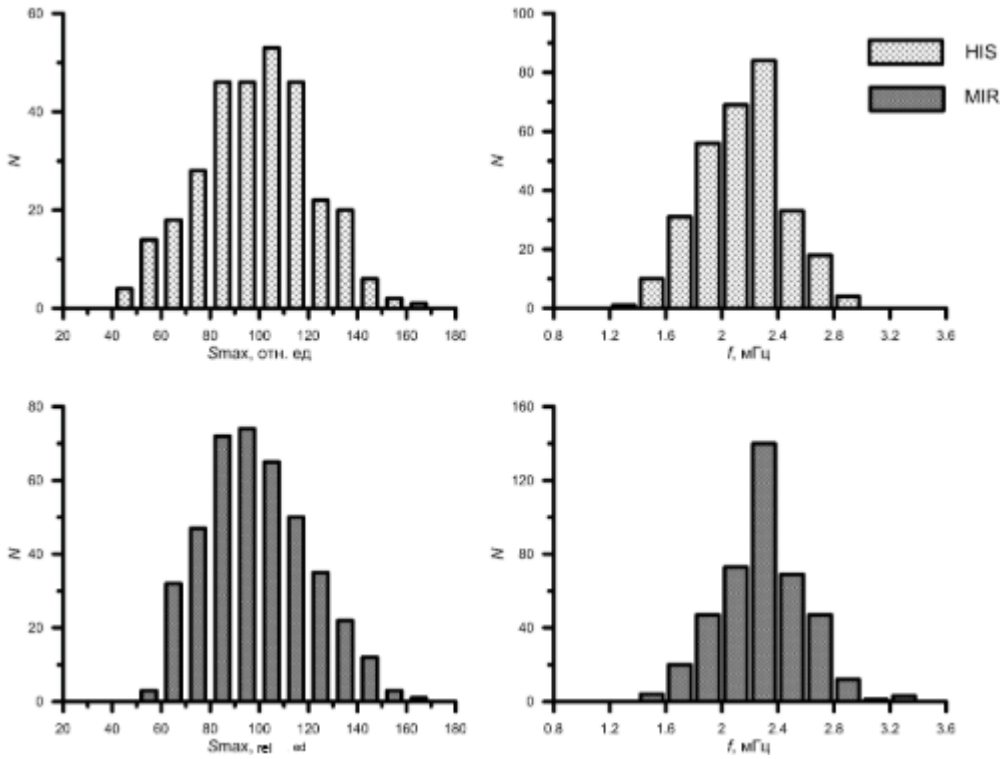
HIS
MIR
N
Smax, отн. ед
f, мГц
Smax, rel ed
f, мГц

Fig. 2.

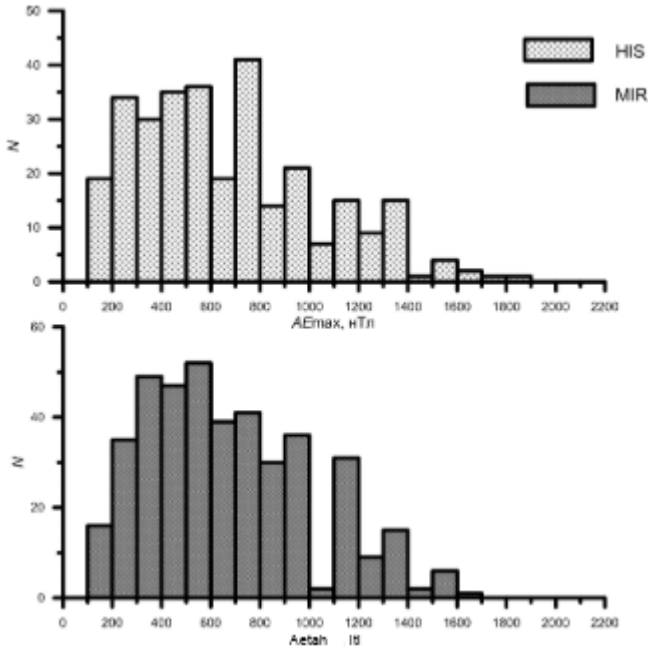
HIS
MIR
N
ΔEmax, нТл
Aetalh, нТл

Fig. 3.

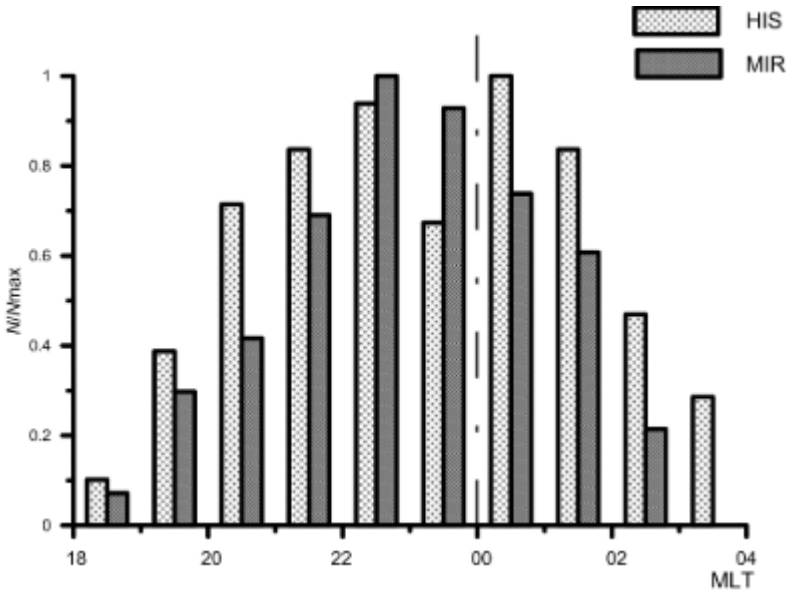
HIS
MIR
1
0.8
0.6
0.4
0.2
0
N/Nmax
18
20
22
00
02
04
MLT

Fig. 4.

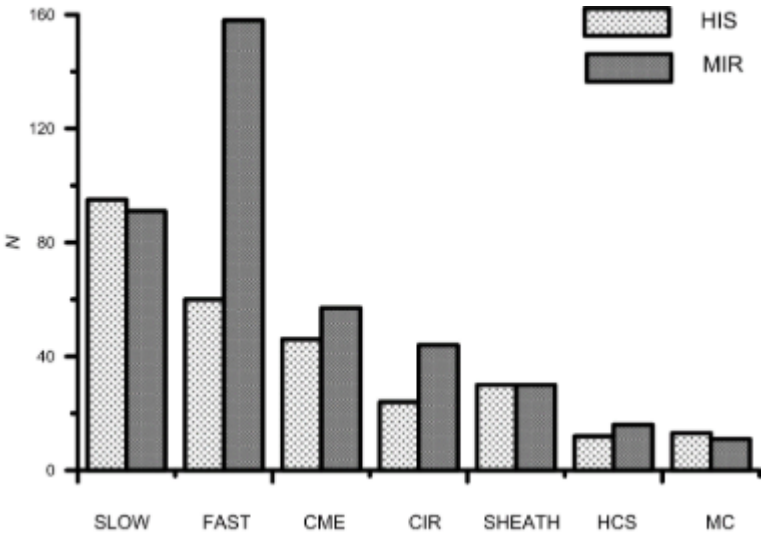
HIS
MIR
160
120
80
40
0
N
SLOW
FAST
CME
CIR
SHEATH
HCS
MC

Fig. 5.

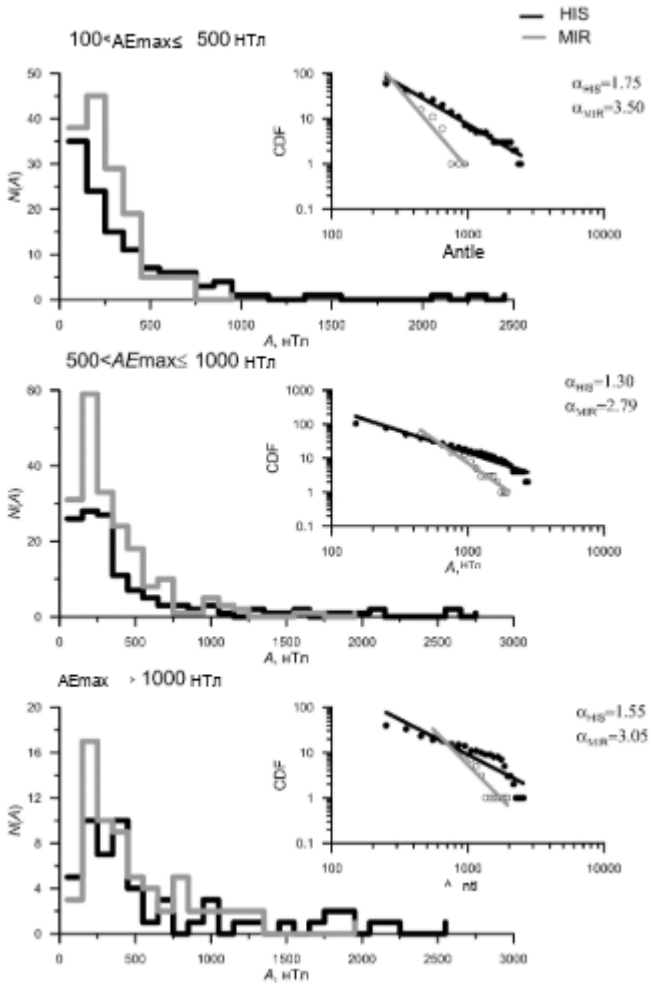
HIS
MIR
100<AEmax≤ 500 нТл
α_{HIS}=1.75
α_{MIR}=3.50
N(A)
A, нТл
CDF
Antle
500<AEmax≤ 1000 нТл
α_{HIS}=1.30
α_{MIR}=2.79
AEmax > 1000 нТл
α_{HIS}=1.55
α_{MIR}=3.05

Fig. 6.

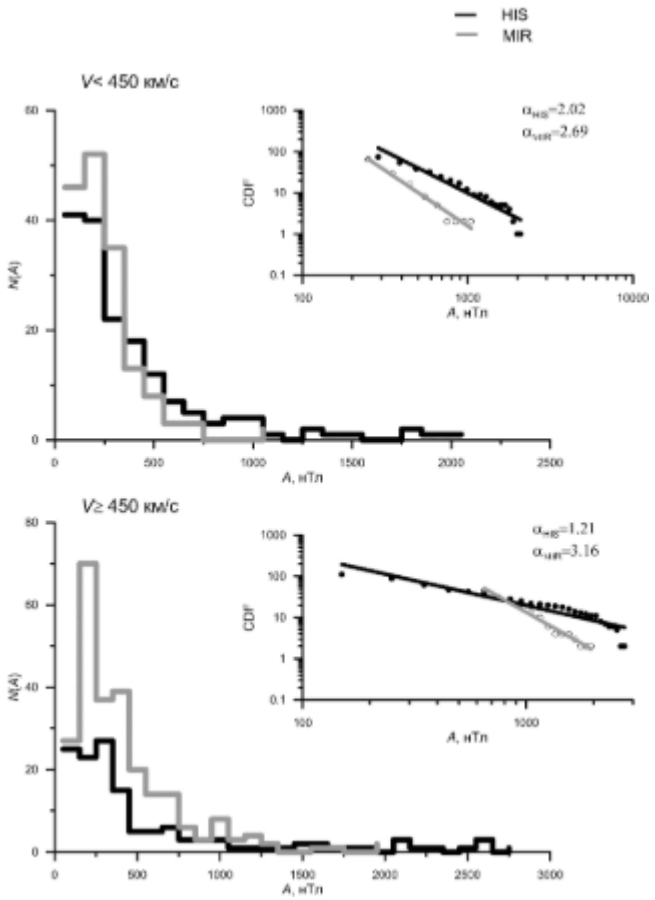
HIS
MIR
V< 450 км/с
α_{HIS}=2.02
α_{MIR}=2.69
N(A)
CDF
A, нТл
V≥ 450 км/с
α_{HIS}=1.21
α_{MIR}=3.16
N(A)
CDF
A, нТл

Fig. 7.

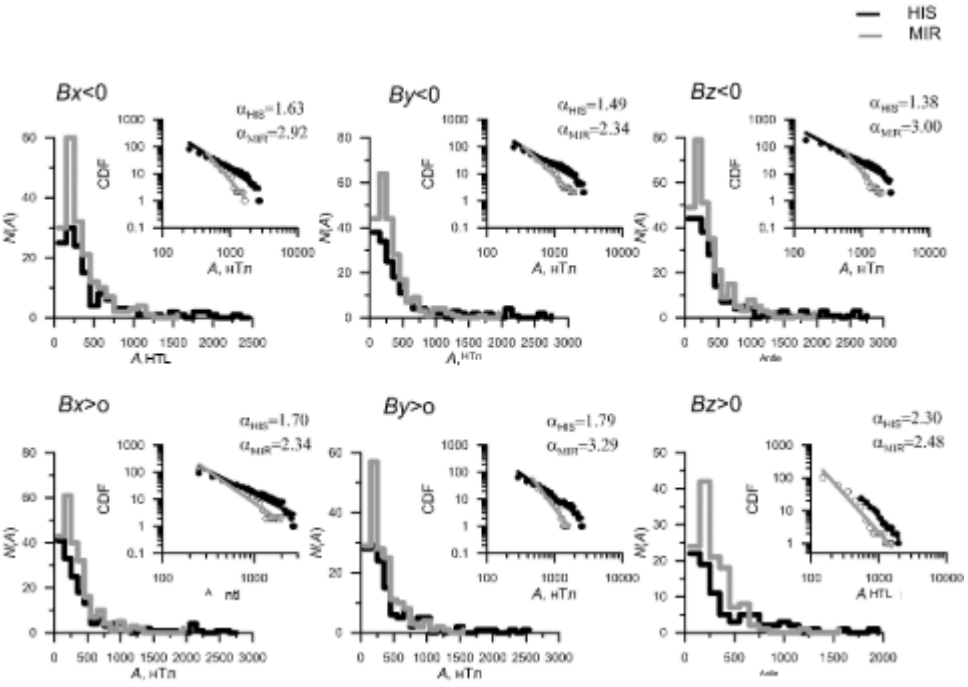
HIS
MIR
Bx<0
α_{HIS}=1.63
α_{MIR}=2.92
By<0
α_{HIS}=1.49
α_{MIR}=2.34
Bz<0
α_{HIS}=1.38
α_{MIR}=3.00
Bx>0
α_{HIS}=1.70
α_{MIR}=2.34
By>0
α_{HIS}=1.79
α_{MIR}=3.29
Bz>0
α_{HIS}=2.30
α_{MIR}=2.48
N(A)
CDF
A, нТл

Fig. 8.

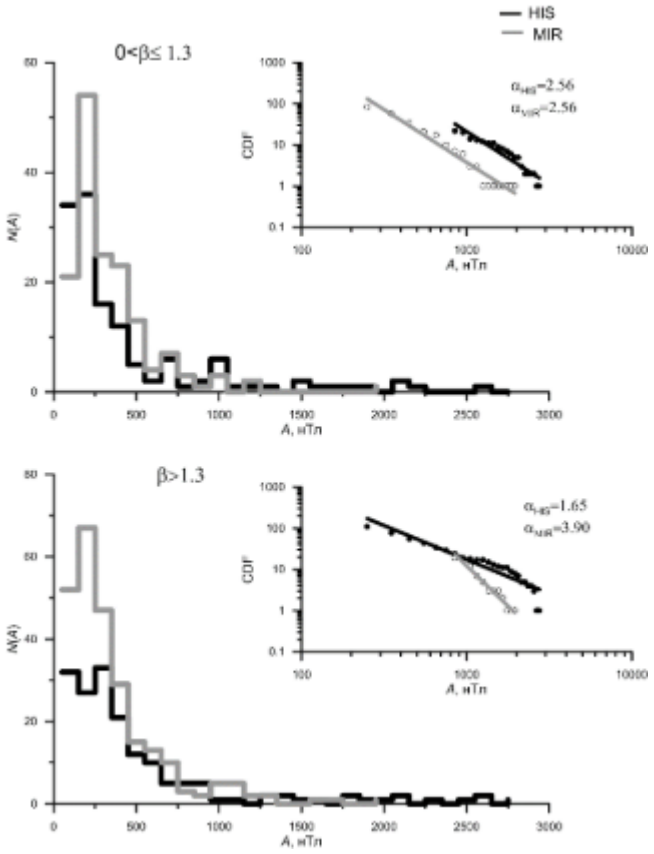
HIS
MIR
0<β≤ 1.3
N(A)
A, нТл
CDF
α_{HIS}=2.56
α_{MIR}=2.56
β>1.3
α_{HIS}=1.65
α_{MIR}=3.90

Fig. 9.